






RESEARCH ARTICLE | JUNE 03 2024

Arrested states in colloidal fluids with competing interactions: A static replica study

Jean-Marc Bomont   ; Giorgio Pastore; Dino Costa  ; Gianmarco Munaò  ; Gianpietro Malescio; Santi Prestipino 



J. Chem. Phys. 160, 214504 (2024)

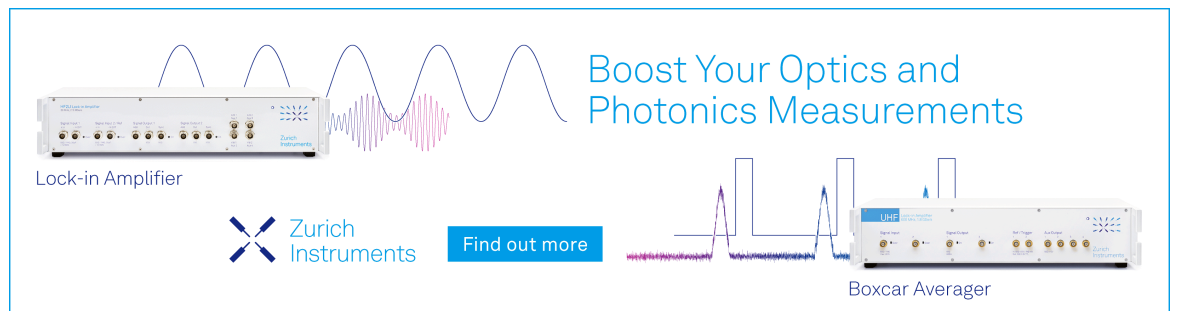
<https://doi.org/10.1063/5.0208117>



View
Online




Export
Citation



Boost Your Optics and
Photonics Measurements

Lock-in Amplifier

 Zurich
Instruments

[Find out more](#)

Boxcar Averager

Arrested states in colloidal fluids with competing interactions: A static replica study

Cite as: J. Chem. Phys. 160, 214504 (2024); doi: 10.1063/5.0208117

Submitted: 13 March 2024 • Accepted: 13 May 2024 •

Published Online: 3 June 2024



View Online



Export Citation



CrossMark

Jean-Marc Bomont,^{1,a)} Giorgio Pastore,² Dino Costa,³ Gianmarco Munaò,³ Gianpietro Malescio,³ and Santi Prestipino³

AFFILIATIONS

¹ Université de Lorraine, LCP-A2MC, UR 3469, 1 Bd. François Arago, Metz F-57078, France

² Dipartimento di Fisica, Università degli Studi di Trieste, Strada Costiera 11, 34151 Grignano (Trieste), Italy

³ Dipartimento di Scienze Matematiche e Informatiche, Scienze Fisiche e Scienze della Terra, Università degli Studi di Messina, Viale F. Stagno d'Alcontres 31, 98166 Messina, Italy

^{a)} Author to whom correspondence should be addressed: jean-marc.bomont@univ-lorraine.fr

ABSTRACT

We present the first systematic application of the integral equation implementation of the replica method to the study of arrested states in fluids with microscopic competing interactions (short-range attractive and long-range repulsive, SALR), as exemplified by the prototype Lennard-Jones–Yukawa model. Using a wide set of potential parameters, we provide as many as 11 different phase diagrams on the density (ρ)–temperature (T) plane, embodying both the cluster-phase boundary, $T_C(\rho)$, and the locus below which arrest takes place, $T_D(\rho)$. We describe how the interplay between T_C and T_D —with the former falling on top of the other, or the other way around, depending on thermodynamic conditions and potential parameters—gives rise to a rich variety of non-ergodic states interspersed with ergodic ones, of which both the building blocks are clusters or single particles. In a few cases, we find that the T_D locus does not extend all over the density range subtended by the T_C envelope; under these conditions, the λ -line is within reach of the cluster fluid, with the ensuing possibility to develop ordered microphases. Whenever a comparison is possible, our predictions favorably agree with previous numerical results. Thereby, we demonstrate the reliability and effectiveness of our scheme to provide a unified theoretical framework for the study of arrested states in SALR fluids, irrespective of their nature.

Published under an exclusive license by AIP Publishing. <https://doi.org/10.1063/5.0208117>

I. INTRODUCTION

Past decades have witnessed a growing interest in the role played by the interparticle interactions in controlling the structure and dynamics of colloidal dispersions—see Refs. 1 and 2 for extensive reviews. Despite being very complex in nature and number of components, such fluids can often be described by means of simple effective, one-component microscopic models.^{3,4} In this respect, it has been well established since the work of van der Waals that fluids interacting via excluded volume plus an isotropic attractive contribution of not too narrow range undergo, at low-enough temperatures, a gas–liquid phase separation.^{5,6} When a further long-range repulsion is added, the situation may change: gas–liquid separation can be preempted by the onset of a microphase separation⁷ in which the system organizes itself into finite-size domains, thus forming a

density-modulated phase. Indeed, experiments, theory, and simulation have demonstrated that, when spherical particles are endowed with a short-range attraction (SA) and a screened electrostatic repulsion at larger distances (LR), various aggregates are formed, whose size and shape crucially depend on the balance between attraction and repulsion.

SALR fluids exhibit a rich variety of phases and microphases not observed in simple fluids governed by Lennard-Jones-like interactions. In particular, one of the most interesting features of SALR fluids is the existence of a cluster microphase, emerging at a sufficiently low temperature, T_C , generally depending on the density ρ . This microphase—resulting from the competition between attraction and repulsion over distinct length scales—has been observed in experiments, as well as in molecular simulations; see, for instance, Refs. 8 and 9. In addition, the cluster microphase of various SALR

models has been the subject of a number of theoretical studies aiming to assess integral equation predictions against numerical simulations; see, for example, Refs. 7 and 10–17.

Eventually, at a temperature lower than the onset of the cluster phase, dynamically arrest may supersede a thermodynamic transition, along the so-called λ -line, between the cluster fluid and a cluster crystal.¹⁸

At the structural level, the ubiquitous signature of the presence of aggregates is the appearance of a low- q peak in the structure factor $S(q)$, located at a wavevector q_c much smaller than the location of the main peak, in turn corresponding to the nearest-neighbor distance. Initially, at the very onset of the low- q peak, the fluid is said to experience an intermediate-range order, IRO.¹⁹ As the temperature goes down and $S(q_c)$ becomes progressively larger, Godfrin *et al.*²⁰ proposed that the equilibrium cluster phase forms when $S(q_c)$ attains the threshold value ≈ 2.7 . This heuristic criterion recalls the well-known Hansen–Verlet freezing rule for simple fluids.²¹ In parallel, Bollinger and Truskett¹⁶ considered the width, rather than the height, of $S(q_c)$, proposing that clusters form when the thermal correlation length ξ_T exceeds the Debye screening length ξ_D ; usually, the latter criterion performs well, at least for large enough screening lengths. More recently, two of us showed that also local, real space correlations—beside the commonly studied structure factor—convey precise information about the clustering process.^{22–24}

In recent years, dynamical arrest in colloidal and, more generally, in soft matter fluids has gained increasing attention.⁹ As for SALR models, much effort has been devoted to clarify the dynamical behavior at high densities,^{2,8} where dynamical arrest, commonly identified as a glass transition, takes place. In addition, there is a special kind of low-density arrested state that is uniquely found in SALR models, below $T_C(\rho)$: the “Wigner glass of clusters,”²⁵ originating from the dominant role of the electrostatic repulsion. In this case, clusters become themselves the building blocks of the arrested state. A Wigner glass of clusters has been found in simulations^{26,27} and experiments²⁸ and also confirmed by mode coupling theory²⁹ in the two-Yukawa SALR model.³⁰ At intermediate densities, in between these two glassy states, SALR systems are known to exhibit, as most colloidal systems do, a gel phase characterized by a network-like structure. Such percolating states have as constituting units either clusters (as in the Wigner glass, and, therefore, they are referred to as cluster-percolated states) or particles (random-percolated states), according to whether thermodynamic conditions fall within the $T_C(\rho)$ envelope or not.²⁰ Recently, the description of dynamical arrest processes in SALR models has been tackled^{31,32} in the framework of the non-equilibrium SCGLE (self-consistent generalized Langevin equation) theory.³³ This approach aims to distinguish between ergodic and non-ergodic states and has been already applied to different fluids with discrete interactions like hard-sphere,³⁴ square-well,³⁵ or the Yukawa potential.^{36,37} It is based on the calculation of a so-called localization length, $\gamma(\rho, T)$; ergodic and non-ergodic states are identified according to whether γ exhibits a diverging or a finite value, respectively.

Notwithstanding progress in the field, dynamical arrest in SALR fluids is still a challenging testbed for theory and experiments. In particular, it is not clear whether arrested states like a Wigner glass or a gel can be described in a unified theoretical framework together with ordinary glasses.

An elegant way, proposed long ago by Franz and Parisi,^{38–40} to detect at large packing fractions the onset of an arrested state in standard fluids is the “Replica Method,” which has since then given rise to many studies—see Refs. 41 and 42 for extensive reviews. The “annealed” version of the method consists in monitoring the evolution of a particle system, weakly coupled to one copy of it, as the temperature is lowered.^{43–45} Recently, some of us have explored in different directions the integral equation implementation of the replica formalism.^{46–53} Briefly speaking, the integral equations connecting pair correlation functions and pair potentials are implemented for a homogeneous mixture of clones (replicas) of the same system. The inter-replica pair correlation function $g'(r)$ leads directly to the overlap (or similarity) Q between the copies. The quantities $g'(0)$ and Q represent order parameters of the Random First Order Transition (RFOT) theory: upon lowering the temperature, $g'(0)$ and Q may undergo a discontinuous jump (dj) at a critical temperature $T_{dj}(\rho)$, signaling a broken translational symmetry of the two-replica system. Such a scenario points to the existence of a liquid (L) phase and an “ideal” glass phase (G_2), in agreement with the original replica method formulation. In addition, also an additional branch of glass solutions (G_1) is found.⁴⁶

The common highest temperature at which G_1 and G_2 phases survive is the so-called dynamical transition temperature T_D , above which the system is in the L phase. More recently, to make contact with the Mézard–Parisi results,⁵⁴ following the Monasson prescription,⁵⁵ we have adapted our search protocol, previously applied to the case of $m = 2$ replicas, to a continuously varying number m of weakly coupled replicas (with m possibly lower than 1) within the framework of the hypernetted chain (HNC) integral equation.⁵² The equilibrium properties of the original, i.e., non-replicated, system are obtained in the $m \rightarrow 1$ limit.

In this paper, we use our simplified replica formalism in the annealed version to search for the existence of arrested states in SALR fluids. To this purpose, we use the prototype LJY potential, formed by a generalized $(2\alpha, \alpha)$ Lennard-Jones potential,⁵⁶ accounting for the short-range attraction, plus a repulsive screened electrostatic Yukawa term, with strength A and decay length ξ_D . For a wide set of (α, A, ξ_D) parameters, we map out the cluster phase boundary $T_C(\rho)$ —as identified by $S(q_c) \approx 2.7$ ²⁰—together with the dynamical arrest locus $T_D(\rho)$. In this way, we present a systematic exploration of how the combination of attraction and repulsion in the microscopic interaction influences the interplay between clustering and arrested states. The present study demonstrates the reliability of our implementation of the integral equation approach to the replica theory as a tool to identify the onset of arrested states in SALR models, whatever their nature.

The rest of this paper is organized as follows: In Sec. II, we review the essentials of our implementation of the replica method. In Secs. III–V, we present our results. Specifically, attention is paid to the role played by the amplitude A of the Yukawa tail in Sec. III. In Sec. IV, we analyze and compare the phase diagrams obtained by systematically increasing the exponent α in the LJY potential; in Sec. IV B, we pursue a further validation of our approach against molecular dynamics results available from previous studies.^{9,27} To make connection with experiments, we study in Sec. V a LJY parameterization suitable to model a realistic colloidal solution;⁵⁷ again, we compare our predictions with previous simulation data.^{31,58} Finally, in Sec. VI, we present our conclusions. The Appendix is devoted to a

further validation of our approach against the glass phase of the standard Lennard-Jones fluid, as calculated within the more complex formalism of Ref. 59.

II. MODEL AND THEORETICAL BACKGROUND

We model the SALR interaction as a combination of the generalized $(2\alpha, \alpha)$ Lennard-Jones potential and a screened Coulomb interaction, accounted for by a repulsive Yukawa potential. Hence, the LJY pair potential reads

$$v_{\text{LJY}}(r) = 4\epsilon \left[\left(\frac{\sigma}{r} \right)^{2\alpha} - \left(\frac{\sigma}{r} \right)^\alpha \right] + A \frac{\exp[-r/\xi_D]}{r/\xi_D}, \quad (1)$$

where r is the interparticle distance, σ is the particle diameter, ϵ is the strength of the short-range attraction, and A is the strength of the long-range repulsion, related to the square of the effective electric charge of a colloidal particle;^{60,61} finally, ξ_D is the electrostatic Debye screening length in units of σ . In reduced units, the temperature is expressed as $T^* = k_B T/\epsilon$, where k_B is the Boltzmann constant, while the reduced density is defined as $\rho^* = \rho\sigma^3$ with ρ being the number density of the system.

For clarity, the interaction potential will be indicated as $\text{LJY}(\alpha, A, \xi_D)$, where it is implied that A and ξ_D are given in units of ϵ and σ , respectively. The set of all $[\alpha, A, \xi_D]$ values considered in this work, amounting to a total of 11 different LJY models, is reported in Table I.

In our theoretical framework, we consider a system of m identical replicas of the original LJY fluid. Atoms belonging to the same replica interact through $v_{\text{LJY}}(r)$, but at the effective temperature $T_{\text{eff}}^* = T^*/m$ [equivalently, $v_{\text{LJY}}(r)$ is replaced by $mv_{\text{LJY}}(r)$], while atoms belonging to different replicas are weakly coupled to each other through a short-range inter-replica attraction of the following form:⁶²

$$v'(r) = -\epsilon' \left[\frac{c^2}{r^2 + c^2} \right]^6 = -\epsilon' w(r). \quad (2)$$

The parameter c is chosen to be 0.3σ , to ensure that an atom of a given replica can at most interact with one single atom of another replica. Notice that the exact form of $v'(r)$ is irrelevant since we shall eventually be interested in the limit $\epsilon' \rightarrow 0$. Such a symmetric m -component “mixture” is characterized by only two pair correlation functions: the intra-replica $g(r)$ and the inter-replica $g'(r)$, regardless of the value of m . Given that $h(r) = g(r) - 1$ and $h'(r) = g'(r) - 1$, the pair correlation functions are related to the corresponding direct correlation functions $c(r)$ and $c'(r)$ via the Ornstein–Zernike relations as follows:^{5,6}

$$h(r) = c(r) + \rho c(r) \otimes h(r) + (m-1)\rho c'(r) \otimes h'(r), \quad (3a)$$

$$h'(r) = c'(r) + c(r) \otimes h'(r) + \rho c'(r) \otimes h(r) + (m-2)\rho c'(r) \otimes h'(r), \quad (3b)$$

where \otimes denotes a three-dimensional convolution product. These relations must be supplemented by closure relations, which, in the HNC approximation, read^{5,6}

$$g(r) = \exp[-\beta_{\text{eff}} v(r) + h(r) - c(r)], \quad (4a)$$

$$g'(r) = \exp[-\beta_{\text{eff}} v'(r) + h'(r) - c'(r)], \quad (4b)$$

with $\beta_{\text{eff}} = 1/T_{\text{eff}}^*$. Equations (3) and (4) hold for any m , including non-integer values and $m < 1$.

Among simple closures, HNC combines a good overall accuracy and the automatic fulfillment of the virial-energy thermodynamic consistency, a property not shared by other schemes, for instance, Percus–Yevick and mean spherical approximation.⁶ Its good performances in predicting the structural properties of SALR fluids were demonstrated in several previous studies.^{11,15,18,63–65} Moreover, HNC is the theory more extensively tested for the replica method at issue, with a positive comparison with more sophisticated integral-equation approaches.^{47–49}

The structural properties of the liquid phase are computed by considering fully decoupled replicas [i.e., by setting $\epsilon' = 0$ in Eq. (2)], which, in turn, implies $h'(r) = c'(r) = 0$. Meanwhile, for finite values of ϵ' , the attraction between atoms of different replicas favors configurations corresponding to the same local free energy minimum. This tendency can be quantified by the order parameter

$$Q = 4\pi\rho \int_0^\infty g'(r) m w(r) r^2 dr. \quad (5)$$

A complementary order parameter is provided by $g'(r=0)$: upon lowering T_{eff}^* , in the absence of inter-replica coupling [$\epsilon' = 0$], we get $g'(0) = 1$, while, for finite ϵ' , a central peak in $g'(r)$ is expected to build up at $r = 0$.⁴⁷

At a given temperature T_{eff}^* , our search protocol consists in solving the set of HNC equations (3) and (4) for $g(r)$ and $g'(r)$, starting from an initial finite value of the inter-replica coupling ϵ' . Then, we follow the evolution of the order parameters Q and $g'(0)$ upon gradually reducing ϵ' . If, in the limit $\epsilon' \rightarrow 0$, the order parameters take their “random” (or uncorrelated) values Q_{ran} [as calculated from Eq. (5) with $g'(r) = 1$] and $h'(0) = 0$, then the thermodynamic state at T_{eff}^* corresponds to the L phase. Meanwhile, if in the same limit “non-trivial” $Q \gg Q_{\text{ran}}$ and $g'(0) \gg 1$ are recorded, then the system is in an arrested state, where replicas are, *a priori*, all equally trapped within the same minimum of the free energy landscape. Taking the limit $m \rightarrow 1$ (i.e., $T_{\text{eff}}^* \rightarrow T^*$) allows us to recover the properties of the non-replicated system at the real reduced temperature T^* .⁵⁵ This process can be repeated for any number of thermodynamic states.

We recall that our earlier calculations^{46,47,49,52} pointed to the existence of two glass-like solutions, namely the “ideal” glass phase G_2 , and the previously undetected branch of solutions G_1 . While replicas remain trapped in the same free-energy minimum in the G_2 phase, the G_1 solution still lacks a precise identification. We may say, however, that the presence of two glassy phases is justified by the fact that—in the standard picture coming from mean field models—the glass transition is related to the appearance of many metastable glassy states in addition to the “ideal” one.⁶⁶ In particular, there are two “types” of metastability: the first one is the metastability of both G_1 and G_2 phases with respect to crystallization. The second type is provided by the existence of G_1 glassy states, which have higher excess free energy compared to the glassy state of the lowest excess free energy (the “ideal” one), and, consequently, the former states are metastable with respect to the latter. Indeed, for both soft spheres^{47–49} and Lennard-Jones atoms,⁵¹ G_1 and G_2 solutions have been shown to coexist over identical ranges of densities

TABLE I. Plan of the $[\alpha, A, \xi_D]$ sets studied in this work. Models LJY(6, A, 2), LJY(α , 0.2, 2), and LJY(18, A, 0.5) are analyzed in Secs. III, IV and V, respectively. The model LJY(18, 8, 0.5) is named LJY_E in Sec. V. The pure LJ is studied in the Appendix. For quick reference, in the last column, we indicate the figures in the text relative to each model.

Model	α	A/ε	ξ_D/σ	Figures
LJY(6, A, 2)	6	$\left\{ \begin{array}{l} 0.20 \\ 0.65 \end{array} \right.$	2.0	1–5 1 and 5
LJY(α , 0.2, 2)	$\left\{ \begin{array}{l} 12 \\ 18 \\ 24 \\ 100 \end{array} \right.$	0.20	2.0	6 6 6 6–9 and 11
LJY(18, A, 0.5)	18	$\left\{ \begin{array}{l} 8.00 \\ 7.80 \\ 7.30 \\ 6.70 \\ 6.30 \end{array} \right.$	0.5	9, 11, and 12 10 10 10 10
Pure LJ	6	0.00	0.0	13 and 14

and temperatures. The common highest temperature at which G_1 and G_2 still survive is identified as the dynamical transition temperature T_D , above which the system switches from the glass phase to the L phase. In the rest of this paper, in order to distinguish the inter-replica pair correlation functions corresponding to G_1 and G_2 phases, non-trivial solutions $g'(r)$ are accordingly renamed as $g'_1(r)$ and $g'_2(r)$.

We have solved numerically the coupled HNC equations for $h(r)$ and $h'(r)$, using the very efficient Gillan iterative algorithm.⁶⁷ We verified the robustness of our predictions against several resolutions Δr of the spatial grid and a corresponding total number N_g of grid points, so as to keep the overall range in direct and reciprocal space large enough and the grid spacing small enough, to minimize truncation and discretization errors. In practice, N_g has never been smaller than 4097 and Δr has never been larger than 0.01 σ .

III. LJY MODELS WITH FIXED LJ ATTRACTION

A. General aspects

To assess our predictions for T_D against those available from the more complex formalism of Ref. 59, we have initially examined the standard Lennard-Jones fluid [i.e., Eq. (1) with $\alpha = 6$ and $A = 0$] at high densities. The results of this analysis are reported in the Appendix, where, moreover, we take the opportunity to present several peculiar aspects of our formalism in detail.

Turning to the full LJY interaction, we begin to leave $\alpha = 6$ unchanged in Eq. (1), with parameters of the repulsive Yukawa tail $A = 0.2\varepsilon$ and $\xi_D = 2\sigma$. The corresponding LJY(6, 0.2, 2) potential is displayed in Fig. 1 (black line).

First, we compute the temperature $T_C(\rho)$ corresponding to $S(q_c) \approx 2.7$.²⁰ Next, we apply our search protocol for $T_D(\rho)$ with $m = 0.8$, $\varepsilon'_0 = 0.1\varepsilon$, and $c = 0.3\sigma$ at the fixed density $\rho^* = 1$. By lowering

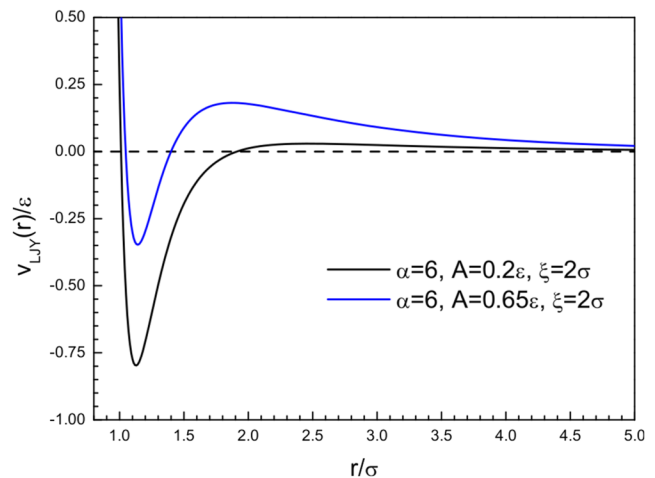


FIG. 1. LJY(6, 0.2, 2) (black) and LJY(6, 0.65, 2) (blue) potentials.

the temperature, the arrested scenario for LJY is found to be identical to LJ, with two successive discontinuous jumps at the effective temperatures $T_{dj1}^* = 0.18$ and $T_{dj2}^* = 0.155$. Taking the limits $\varepsilon' \rightarrow 0$ and $m = 1$ allows us to obtain both $g'_1(r)$ and $g'_2(r)$ solutions. In order to obtain the dynamical transition locus $T_D(\rho)$, the density and temperature are varied within each arrested phase.

The $T_C^*(\rho^*)$ and $T_D^*(\rho^*)$ loci are displayed in Fig. 2. We see that the former exhibits a re-entrant concave shape with a maximum located at $[\rho_{C,max}^* \approx 0.23, T_{C,max}^* \approx 0.68]$, above which the fluid is in the IRO state. For temperatures below $T_{C,max}^*$, for increasing density, the fluid moves from an initial IRO state to the cluster phase and then again to the IRO state, indicating that upon compression, the

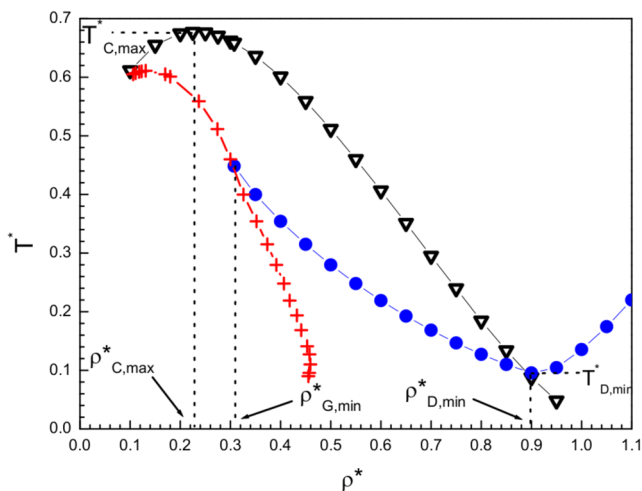


FIG. 2. LJY(6,0.2,2) model. $T_C(\rho)$ (triangles), $T_D(\rho)$ (circles), and the λ -line (crosses). The top of the first locus, falling at $[\rho_{C,\max}^* \approx 0.23, T_{C,\max}^* \approx 0.68]$, and the bottom of the second locus, at $[\rho_{D,\min}^* \approx 0.9, T_{D,\min}^* \approx 0.095]$, are explicitly indicated; the locus $T_D(\rho)$ ends on the lower side at $\rho_{G,\min}^* \approx 0.31$, equally shown.

fluid needs to be progressively cooled in order to attain the cluster phase.

At variance with $T_C(\rho)$, due to its convex shape, $T_D(\rho)$ exhibits a minimum located at $[\rho_{D,\min}^* \approx 0.9, T_{D,\min}^* \approx 0.095]$ and these two lines cross at (ρ_x^*, T_x^*) , a point which, in the present case, almost coincides with $[\rho_{D,\min}^*, T_{D,\min}^*]$.

On opposite sides of $T_{D,\min}^*$, different behaviors occur. In particular, the convex shape of $T_D(\rho)$ implies, for $T^* > T_{D,\min}^*$, the existence of two successive re-entrant arrested states upon compression, intercalated by the liquid phase. This is detailed in Fig. 3, where the evolution of $g'_1(r=0)$ and $g'_2(r=0)$ is reported for two temperatures encompassing $T_{D,\min}^*$. In both cases, starting from $\rho^* = 1$, the density is decreased down to $\rho^* = 0.8$. Along the isotherm $T^* = 0.10$ (i.e., above $T_{D,\min}^*$), $g'_1(r=0)$ and $g'_2(r=0)$ (red lines in Fig. 3) are found to, respectively, increase and decrease, until dropping to their L value 1 at $\rho^* = 0.94$; coherently with the re-entrant behavior just discussed, the opposite trend is observed below $\rho^* = 0.88$. The situation changes along the isotherm $T^* = 0.09$ (i.e., below $T_{D,\min}^*$, blue lines): here, $g'_2(0)$ initially decreases until it reaches a minimum around $\rho^* = 0.92$ and then increases, while $g'_1(0)$ symmetrically exhibits the opposite trend. This feature suggests—together with the crossing with $T_C(\rho)$ —the existence, within the arrested state, of two behaviors of a different nature: one due to particles within the IRO (for $\rho^* \geq 0.92$), and the other being, instead, specific of the cluster phase (for $\rho^* < 0.92$).

Now, we turn to the structural and thermodynamic properties of clustered states below T_D . Figure 4 shows $S(q_c)$ as a function of density along the isotherm $T^* = 0.219$. Upon expansion, $S(q_c)$ increases up to a maximum, then it slightly bends downward, this way following a trend reminiscent of the convex shape of $T_C(\rho)$. As the density is further decreased, $S(q_c)$ exhibits a steep rise to much higher values. This signals the transition from a disordered-pattern to an ordered-pattern cluster fluid, with the ensuing divergence of

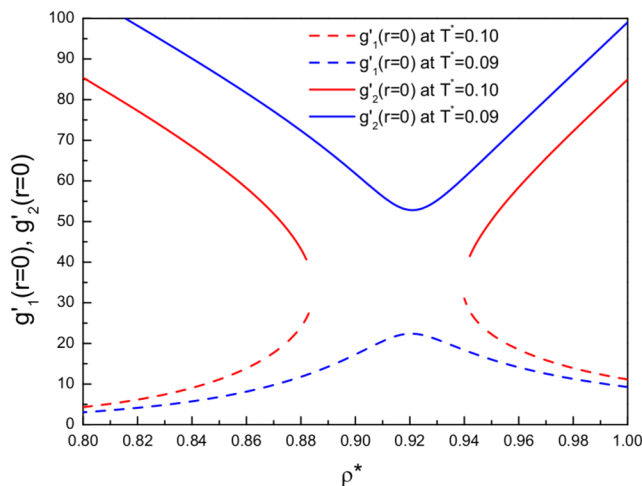


FIG. 3. LJY(6,0.2,2) model. Order parameters $g'_1(0)$ (dashed lines) and $g'_2(0)$ (solid lines), plotted as a function of density, at $T^* = 0.10$ (red) and $T^* = 0.09$ (blue), respectively, falling closely above and below $T_{D,\min}^* = 0.095$.

$S(q_c)$, indicating that the λ -line is reached. In this state, the system minimizes the energy associated with the long-range repulsion by the formation of domains of high density, thus giving rise to mesoscopic patterns. The corresponding shift of q_c toward lower values (not shown) testifies how such domains become more compact as the density decreases. As for the $q \rightarrow 0$ limit of the structure factor, directly related to the compressibility, this property is also shown in Fig. 4. We see that $S(0)$ increases with decreasing density and exhibits a steep rise to much higher values as the λ -line is approached. This suggests a competition between a loss of available space within the domains and a gain in between them, overall giving rise to a fluid with enhanced compressibility. The excess internal energy per particle $\beta U^{\text{ex}}/N$, also shown in Fig. 6, decreases monotonically with decreasing density. It keeps positive until $\rho^* \approx 0.56$ —witnessing how repulsive forces dominate in the fluid—and then turns negative, indicating that particles become, on average, more and more sensitive to the attractive part of the potential; this induces the creation of an increasing number of bonds, again preparing the occurrence of the λ -line.

The above calculations can be repeated for a number of isotherms, so as to map out the whole λ -line. This line is shown in Fig. 2 together with $T_C(\rho)$ and $T_D(\rho)$. We see that the high-density segment of the λ -line falls below T_D , and, therefore, the possibility for it to be attained by the fluid on cooling is preempted by dynamical arrest. Meanwhile, $T_D(\rho)$ does not extend over the whole range of densities, rather terminating on the lower side at $\rho_{G,\min}^* \approx 0.31$, where it crosses the λ -line. The reason is that, since $T_D(\rho)$ increases with decreasing density, we would attain a too high temperature and/or a too low density for a glass state to exist. Under these conditions, the approach to the λ -line is not preempted by arrest, and, therefore, it is within the reach of the clustered fluid; indeed, we can see from Fig. 2 that the temperature at which the λ -line is located rapidly increases as the density is lowered, until it matches the $T_C(\rho)$ locus at $\rho^* \approx 0.1$. In turn, this implies the possibility for the cluster fluid to evolve toward some form of ordered microphases.

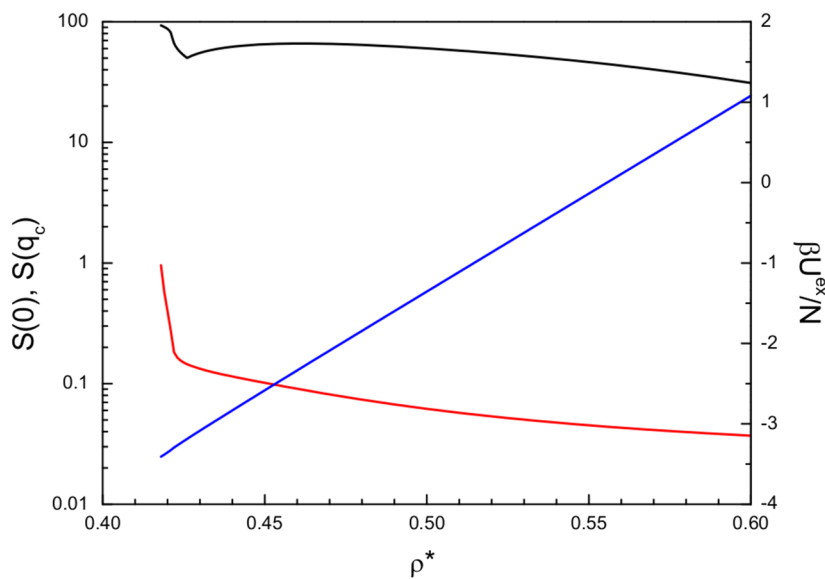


FIG. 4. LJY(6, 0.2, 2) model. $S(q_c)$ and $S(0)$ (black and red lines, respectively; scale on the left) and $\beta U^{\text{ex}}/N$ (blue, right scale) vs ρ^* at $T^* = 0.219$.

To conclude, the attainment of the λ -line is signaled in our framework only indirectly, by the numerical evidence of lack of physical solution of the HNC equations (indeed, the HNC is unable to capture a true divergence).⁶⁸ This implies that a characterization of ordered patterns developing below the λ -line is precluded to our theoretical framework. In addition, it necessarily follows that the λ -line invariably falls at temperatures lower than $T_D(\rho)$ under all thermodynamic conditions for which the existence of an arrest line is predicted by our scheme. As we shall see in the rest of this paper, the present LJY(6, 0.2, 2) parameterization is the only one, among those analyzed in this study, for which dynamical arrest does not occur over the whole density range. Another exception is provided by the LJY(12, 0.2, 2)—discussed in Sec. IV—for which, however, the density range whereupon dynamical arrest does not take place is restricted to a narrow low-density interval. All this considered—all the more so taking into account the “extrapolated” nature of our localization—we limit to the parameterization at issue the only case for which we discuss, by way of example, the behavior of the λ -line.

B. Strengthening the repulsive tail

We investigate how the general scenario presented above changes as the LJY repulsive tail is strengthened and/or the attraction becomes sufficiently short-ranged. As for the first point, we examine the fate of $T_D(\rho)$ as the parameter A is increased from 0.2ϵ to 0.65ϵ , while keeping $\alpha = 6$ and $\xi_D = 2\sigma$ fixed. As can be seen from Fig. 1, this change leads to a shorter and shallower attractive well in the LJY interaction, as well as to a higher and longer repulsive tail.

The phase diagram of LJY(6, 0.65, 2) is shown in Fig. 5, where previous results concerning LJY(6, 0.2, 2) are also shown. Compared to LJY(6, 0.2, 2), $T_C(\rho)$ now shifts to much lower temperatures,

with $T_{C,\text{max}}^* = 0.26$, while $\rho_{C,\text{max}}^* \approx 0.23$ keeps almost unchanged. This results in a cluster phase that extends less toward the high-density side, ending at $\rho^* \approx 0.8$, to be compared with $\rho^* \approx 0.95$ for LJY(6, 0.2, 2). Within the cluster phase, also the locus $T_D(\rho)$ involves lower temperatures and crosses $T_C(\rho)$ at $[\rho_x^* \approx 0.75, T_x^* \approx 0.063]$; therefore, at variance with the previous case, this crossing point no longer coincides with $[\rho_{D,\text{min}}^* \approx 0.8, T_{D,\text{min}}^* \approx 0.06]$. Interestingly, the $T_D(\rho)$ locus turns out to be barely affected by the increase of A in the high density domain $\rho^* > 0.9$, where the fluid experiences IRO conditions. The most important impact on the phase diagram is observed on the low-density side, where, indeed, $T_D(\rho)$ flattens and extends down to $\rho^* = 0.1$. Therefore, increasing A promotes the existence of low-density arrested states, as signaled by the G_1 and G_2 types of solutions.

C. Discussion

The phase behaviors reported in Figs. 2 and 5 reveal a rich picture, with $T_C(\rho)$ and $T_D(\rho)$ alternatively falling one on top of the other, in such a way that the LJY fluid visits a variety of different phases, depending on the relative position of such loci.

All along the density range, the arrested states involve structures in which the building blocks are provided either by clusters (below T_C) or by single particles (as under IRO conditions), and we are able to discriminate between these two structures by studying the interplay between the T_C and T_D loci. When the temperature–density region where clustering occurs is not fully traversed by the arrested line, the cluster fluid is under favorable conditions for an ordered microphase to develop below the λ -line.

According to the generalized phase behavior of Ref. 20, we can reasonably surmise that—once the $T_D(\rho)$ locus extends over the whole density range subtended by $T_C(\rho)$ —a Wigner glass of clusters forming at a low density gives way, somewhere at a higher

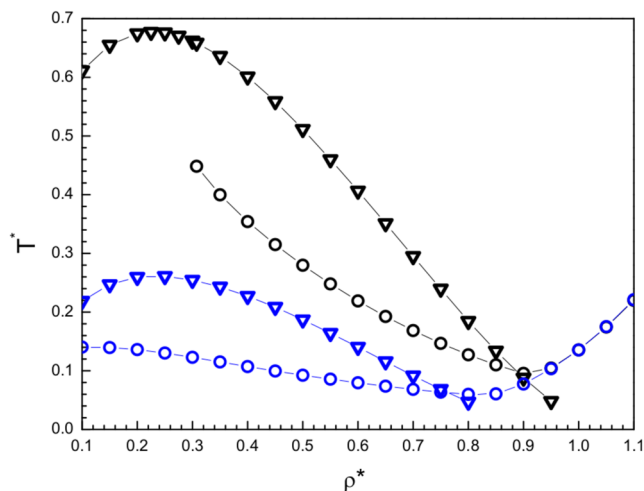


FIG. 5. LJY(6, 0.65, 2) model. $T_C^*(\rho^*)$ (blue triangles) and $T_D^*(\rho^*)$ (blue circles). For the sake of comparison, these curves are plotted together with those relative to LJY(6, 0.2, 2) (black symbols), as redrawn from Fig. 2.

density, to a cluster-percolated network. In this case, we have not been able to find useful indications—neither in terms of structural properties nor in terms of specific features of order parameters—to discriminate between these two different situations. Such difficulties possibly stem from the known similarity of the static properties characterizing both the cluster phase and the gel.^{9,28}

Finally, our scheme captures the features of high-density glassy states, as shown for the standard Lennard-Jones in the Appendix.

In summary, the arrested states of different nature can be gratifyingly predicted within our unified theoretical framework. Sections IV and V will be devoted to a systematic analysis, as different LJY shapes are considered; particular features, concerning specific modelizations and partly departing from the general scenario illustrated above, will be discussed. This survey will provide the occasion for a further assessment of our method against available simulation results.

To conclude, it would be highly desirable to find a “universal” scheme to determine the general properties of SALR phase diagrams. As far as $T_C(\rho)$ is concerned, we recall that—inspired by the so-called extended law of corresponding states (ELCS), formulated by Noro and Frenkel⁷² in the context of short-range attractive models—Godfrin *et al.*²⁰ proposed a similar sort of universal behavior and then validated for a number of different SALR interactions.⁹ Their idea was to consider the attractive part of a given SALR interaction (as obtained by cutting off the repulsive tail) as a “reference” potential and to compute the corresponding gas–liquid coexistence. Then, these authors showed that such a binodal line is a reasonably accurate indicator for the onset of the cluster phase in the original SALR interaction. Admittedly, this result does not ensure the validity of a fully generalized ELCS for systems with competing interactions. Indeed, as for the ELCS of Ref. 72 and for the original van der Waals law in simple liquids, the corresponding states should imply identical thermodynamic and structural properties, but this is not always the case for SALR potentials.⁹ Nevertheless, it would be intriguing

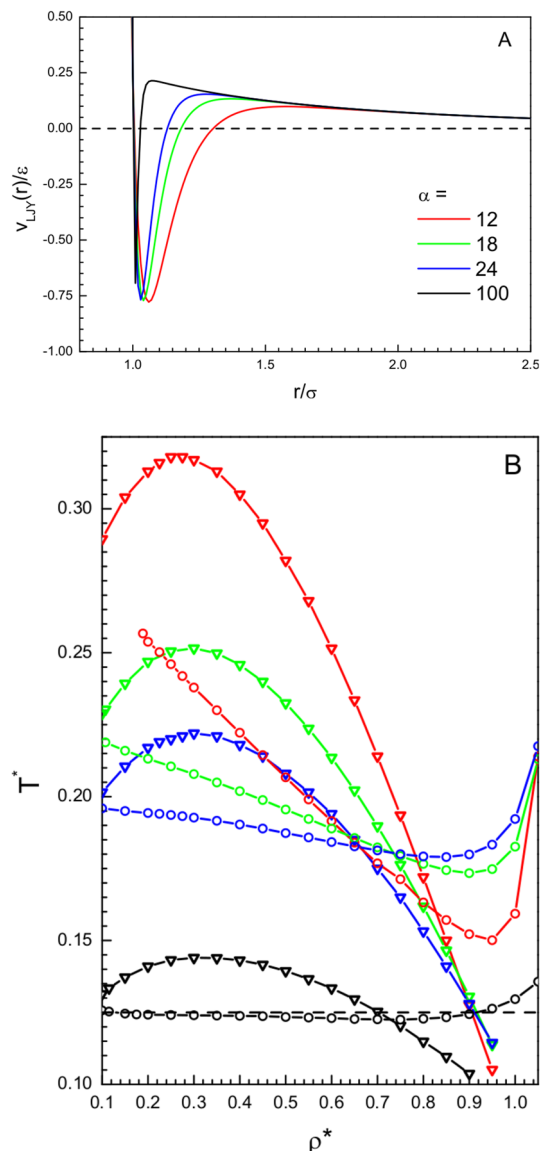


FIG. 6. LJY models with $A = 0.2\epsilon$, $\xi_D = 2\sigma$, and different α , in the legend (a) and corresponding phase diagrams [(b), same color code], in terms of $T_C^*(\rho^*)$ (triangles) and $T_D^*(\rho^*)$ (circles). The dashed line in (b) indicates the isotherm $T^* = 0.125$.

to look for a similar kind of generalized behavior also for the $T_D(\rho)$ line.

IV. LJY MODELS WITH FIXED YUKAWA TAIL

A. Properties for progressively shorter attraction

To examine the influence of the LJ exponent α on the location of arrested states, we fix $A = 0.2\epsilon$ and $\xi_D = 2\sigma$, as in Sec. III, while α is progressively increased from 6 to 12, 18, 24, and 100. In this way, the attractive well is progressively shortened, as shown in Fig. 6(a).

TABLE II. Coordination number, $\langle n \rangle$, and location of the first minimum of $g(r)$, r_{\min} , reported as a function of α , at the relative state $[\rho^* = 0.1, T_C^*(\rho^* = 0.1)]$.

α	$T_C^*(0.1)$	r_{\min}	$\langle n \rangle$
12	0.2895	1.47	2.885
18	0.2288	1.32	2.609
24	0.2015	1.24	2.515
100	0.1314	1.07	2.422

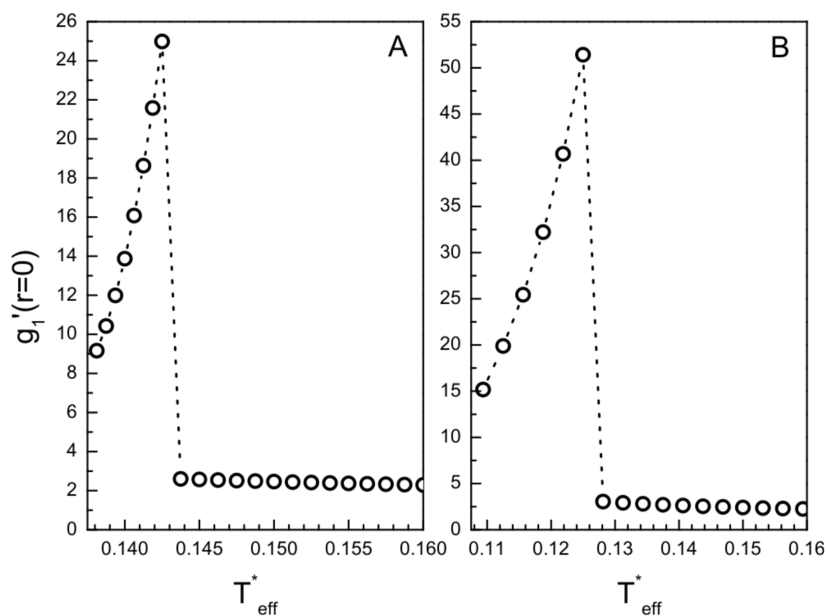
The phase diagrams of pure Lennard-Jones fluids with $\alpha = 12$ and 18 were studied in Ref. 56, demonstrating how they exhibit a rather flat gas–liquid coexistence, in sharp contrast with the case $\alpha = 6$. Moreover, the cluster ground-state properties of LJY($\alpha, 0.2, 2$) were shown to be almost insensitive to α for $\alpha \geq 18$.^{26,69} For such values, a micro-phase separation into clusters exists (see Fig. 9 of Ref. 69).

As for the cluster phase, the shape of $T_C(\rho)$ for all the LJY($\alpha, 0.2, 2$) models in Fig. 6(b) remains qualitatively unchanged, although $T_{C,\max}^*$ decreases with increasing α , while the opposite trend is observed for $\rho_{C,\max}^*$. To assess our predictions, we observe that particles within a cluster, since being caged by many neighbors, are likely to have a local glassy structure (i.e., amorphous with limited mobility), which needs to be sustained by a minimum average coordination number $\langle n_0 \rangle = 2.4$.^{70,71} In Table II, we report $\langle n \rangle$ —as computed by integrating $\rho^* g(r)$ from 0 to its first minimum r_{\min} —as a function of α at $T_C^*(\rho^* = 0.1)$. We find that $\langle n \rangle$ exceeds the threshold (n_0) in all cases, the shorter-range the LJY potential, the closer these two values.

As for the arrested states, we have generally obtained both $g_1'(r)$ and $g_2'(r)$ solutions, except for $\alpha > 28$, where we have only found G_1 -type solutions, the G_2 branch being inaccessible to our approach. However, this is not a serious drawback for the pursuit of our investigation since, as documented before, both G_1 and G_2 types of solutions independently predict, for a given density, the same dynamical-transition temperature. Therefore, $T_D(\rho)$ can be obtained solely from the knowledge of G_1 , as exemplified in Fig. 7 for two specific cases involving low and high densities. The analogies with the features of the dotted-dashed lines in Fig. 13(b) are apparent, and the same discussion applies.

The loci $T_D(\rho)$ corresponding to the LJY($\alpha, 0.2, 2$) models are shown in Fig. 6(b) as well. We see that using a progressively shorter LJY attraction deeply influences the shape of such a locus. On the high-density side, the minimum at $[\rho_{D,\min}^*, T_{D,\min}^*]$ becomes less and less marked until, for $\alpha = 100$, T_D becomes practically flat below T_C , lying around $T^* = 0.125$ independently of the density. At the same time, on the low-density end, $T_D(\rho)$ progressively extends toward lower and lower densities, until covering the whole investigated range for $\alpha > 12$. Moreover, opposite trends are predicted for $T_D(\rho)$ across ρ_x^* . Indeed, for $\rho^* \leq \rho_x^*$, this locus sinks at lower and lower temperatures as α increases, while the opposite occurs at higher densities (at least for $\alpha \leq 24$).

In summary, shortening the LJY attraction hinders the appearance of arrested states made of clusters (Wigner glass or cluster-percolated network) in two complementary ways: first, the density range where $T_D < T_C$ progressively shrinks toward lower and lower densities [ρ_x^* moves to the left in Fig. 8(b)]. Second, increasing cooling is required. Meanwhile, the density range over which a random-percolated state exists is correspondingly extended further with increasing α .

**FIG. 7.** LJY(100, 0.2, 2) model. Order parameter $g_1'(0)$ at $\rho^* = 0.2$ (a) and $\rho^* = 1.1$ (b), under conditions $m = 0.8$, $\epsilon_0' = 0.1\epsilon$, and $c = 0.3\sigma$.

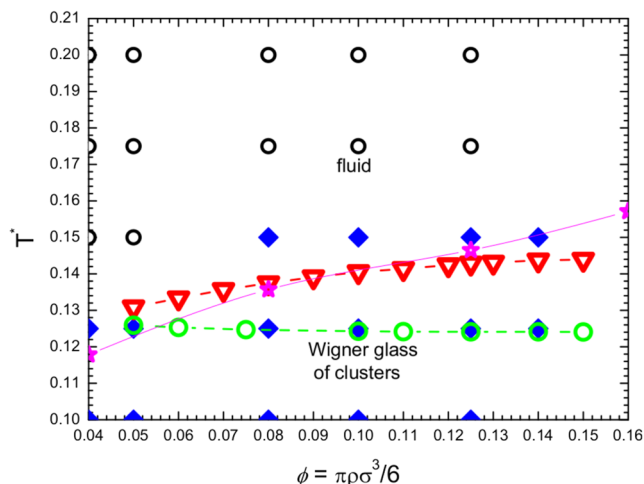


FIG. 8. Low-density phase diagram of the LJY(100, 0.2, 2) model, displaying $T_C^*(\rho^*)$ (triangles) and $T_D^*(\rho^*)$ (green circles). For comparison, MD data from Ref. 27 are also shown: fluid phase (black circles), cluster phase (diamonds), and iso-diffusivity $D/D_0 = 0.1$ line (stars).

B. Comparison with previous simulation studies

Here, we discuss in more detail the features of the LJY model with $\alpha = 100$ and, as before, $A = 0.2\epsilon$ and $\xi_D = 2\sigma$. The study of LJY(100, 0.2, 2) is particularly worth to pursue, since it allows for further validation of our simplified approach against molecular dynamics results available from previous studies.^{9,27}

As for the cluster phase, we recall that a way to establish $T_C(\rho)$, independently of the structural information, consists in computing the cluster size distribution (CSD). Indeed, upon lowering the temperature at fixed density, the point at which the system passes from an IRO to a clustered state is signaled by the appearance of a local maximum in the CSD, indicating the onset of a preferential size of aggregates. In Ref. 9, the CSD calculated for the LJY(100, 0.2, 2) model at the packing fraction $\phi = 0.08$ —corresponding to the reduced density $\rho^* \approx 0.153$ —displays a maximum for $T^* \leq 0.14$ [see Fig. 2(c-ii) therein]. Gratifyingly, our prediction under the same conditions, reported in Fig. 6(b), practically coincides with the simulation datum. A more extended comparison with other CSD results²⁷ is presented in Fig. 8.

As for the arrested states, the approach to these conditions from the equilibrium side was studied by molecular dynamics in Ref. 27. Therein, the authors computed the so-called iso-diffusivity lines, i.e., loci in the phase diagram characterized by a fixed value of the diffusion coefficient. Now, it is known that the shape of iso-diffusivity lines does not change much as the $D \rightarrow 0$ limit is approached, fixing an end point that can be identified with the ideal arrest transition. Therefore, the arrested states are usually thought to develop more or less in parallel to the low- D iso-lines. For the LJY(100, 0.2, 2) model at issue, the D vs T curve has been shown to display a rapid decrease below $T^* = 0.2$, followed by a slower decrease for $T^* \leq 0.125$, which might be considered as the finite- T arrest line,²⁷ also propagating at larger densities. Moreover, at low densities and temperatures, non-percolating states undergo a dynamical arrest

that is realized—because of the cluster–cluster interactions dominating in this regime—through the formation of a Wigner glass of clusters.²⁷

Our predictions for $T_D^*(\rho^*)$, as obtained from G_1 -type solutions, are shown in Fig. 6(b). As already mentioned, this locus turns out to be almost flat below $T_C^*(\rho^*)$, with an approximately constant value close to 0.125, an outcome again in quantitative agreement with the simulation datum just discussed.

In Fig. 8, we replot our predictions for $T_C^*(\rho^*)$ and $T_D^*(\rho^*)$ of the LJY(100, 0.2, 2) model, with a magnification of the low-density portion ($\rho \lesssim 0.3$), where the study of Ref. 27 was focused. We see that our $T_C^*(\rho^*)$ line reasonably follows at low packing fractions the shape of the cluster-phase boundary determined via CSD. For completeness, also our prediction $T_D^*(\rho^*) \approx 0.125$ is shown, together with the iso-diffusivity line $D/D_0 = 0.1$, with D_0 being the bare diffusion coefficient.

V. REALISTIC LJY COLLOIDAL MODEL

A. Phase diagram

We turn to the study of another widely used LJY parameterization, with $\alpha = 18$, $A = 8\epsilon$, and $\xi_D = 0.5\sigma$. The model, referred to in the following as LJY_E, was shown⁵⁸ to closely reproduce the behavior of an experimental charged colloidal solution with added depletion interactions.⁵⁷

In Fig. 9(a), we compare the shapes of LJY_E and LJY(100, 0.2, 2): we see that the attractive well of the former is wider; moreover, if the height of the repulsive barrier is similar, the speed of decay differs, due to the difference in the Debye length ξ_D [the repulsive part of the LJY(100, 0.2, 2) is substantially longer]. Therefore, by comparing the behavior of these two models, we have the opportunity to examine the role played by the electrostatic contribution to the arrested states.

The phase behaviors of LJY_E and LJY(100, 0.2, 2) are shown in Fig. 9(b). As for the clustered state, the shape of $T_C(\rho)$ for LJY_E differs from that observed for previous models, suggesting a more complex cluster phase behavior. Indeed, even though $T_C(\rho)$ shows a maximum, located at [$\rho_{C,\max}^* \approx 0.3$, $T_{C,\max}^* \approx 0.121$], it also exhibits a clear minimum at [$\rho_{C,\min}^* \approx 0.125$, $T_{C,\min}^* \approx 0.113$]. As a result, this locus can be split into two distinct portions, referred to as regime I for $\rho^* < \rho_{C,\min}^*$ and regime II otherwise. In regime II, $T_C(\rho)$ behaves similarly as other LJY models, while regime I, featured by the decrease of T_C with the density, seems to be specific of the LJY_E model.

To perform a further assessment of our HNC predictions, we have calculated T_C^* also within the accurate self-consistent HMSA theoretical approach,⁷³ by adopting the Weeks–Chandler–Andersen scheme to split the interaction potential.⁷⁴ It turns out that HMSA and HNC predictions substantially agree. We are, moreover, confident about the accuracy of $T_C(\rho)$ within regime II, since we have the opportunity to compare with CSD curves:⁹ at $\phi = 0.08$ (i.e., $\rho^* = 0.153$), the CSD starts to exhibit a clear maximum at $T^* \leq 0.12$, in agreement with our HNC prediction $T_C^*(0.153) = 0.116$. Moreover, the $S(q_c)$ obtained from simulation for $\phi = 0.125$ and 0.16 (with $\rho^* = 0.239$ and 0.305, respectively) at $T^* = 0.12$ exceeds the threshold value 2.7,⁵⁸ again in agreement with our predictions. Notice, however, that, within regime I, the CSD suggests at $\phi = 0.04$ ($\rho^* = 0.076$)

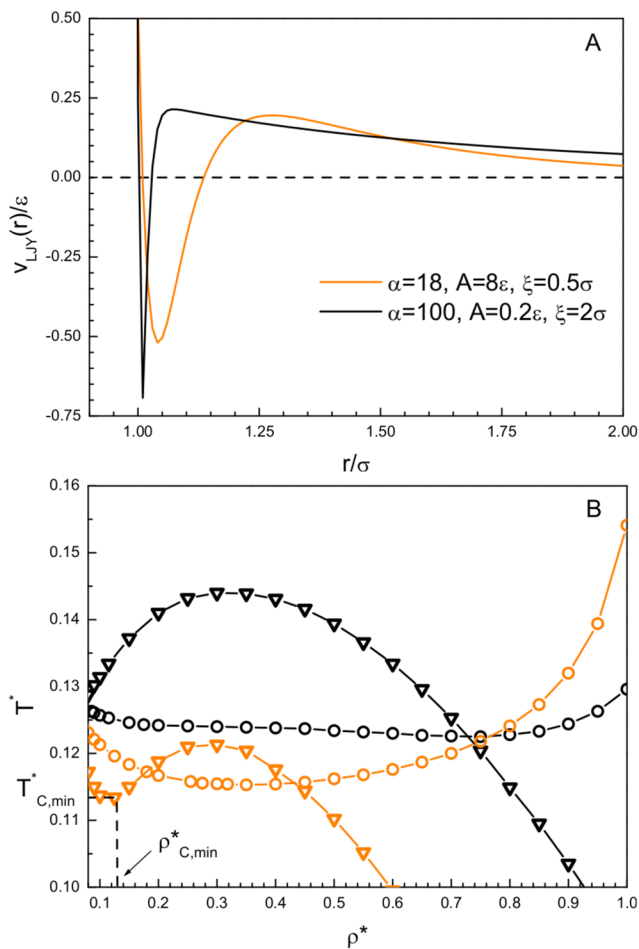


FIG. 9. (a) The LJY_E potential (orange), as compared with LJY(100,0.2,2) (black). (b) Corresponding phase diagrams with the same color code, displaying $T_C^*(\rho^*)$ (triangles) and $T_D^*(\rho^*)$ (circles).

a cluster phase at $T^* = 0.10$,⁵⁸ a temperature much lower than that predicted by HNC.

Therefore, since we are confident that our HNC prediction for the height $S(q_c)$ is reasonably accurate, we are left with the suspect that for LJY_E, the correspondence $T_C \leftrightarrow S(q_c) \approx 2.7$ ²⁰ is flawed in the low-density regime I, all the more so because the opposite implies questioning the well-established proximity between T_C and the liquid–vapor binodal of the corresponding reference fluid, discussed in Sec. III C. While deserving further investigation, this issue cannot be solved within our theoretical approach and is, therefore, deferred to future studies. Before concluding, we anticipate two considerations, which are to be detailed in the next paragraphs. First, the upward bending of T_C in regime I is also present, even more pronounced, for a whole family of LJY_E parameterizations, obtained from the original one by decreasing A ; this again calls for a deeper understanding of the whole topic. Second, even if we regard $S(q_c) \approx 2.7$ as signaling the highest temperature for the existence of the clustered state, we shall see that, in the low-density regime I, T_D falls

TABLE III. Coordination number $\langle n \rangle$ vs $\rho^* \leq \rho_{\times 1}^*$ along $T_D^*(\rho^*)$ for LJY_E.

ρ^*	$T_D^*(\rho^*)$	$\langle n \rangle$
0.080	0.1231	2.459
0.090	0.1221	2.620
0.100	0.1213	2.765
0.125	0.1196	3.110
0.150	0.1184	3.422
0.180	0.1173	3.759

invariably above this threshold, with implications on the nature of the arrested state for the LJY_E family under scrutiny.

We now drive our attention to the dynamical arrest transition. Contrary to LJY(100,0.2,2), for LJY_E, we have found both G_1 and G_2 solutions. Noticeably, $T_D(\rho)$ differs from the previous ones in that it crosses $T_C(\rho)$ twice, at $\rho_{\times 1}^* \approx 0.18$ and $\rho_{\times 2}^* \approx 0.45$; see Fig. 9(b). As a result, the area subtended by the two loci turns out to be very narrow, with the density range within which clusters may exhibit arrested states narrowed accordingly. Under these conditions, therefore, once clusters have formed, a feeble decrease in temperature is sufficient to let them arrest, the more so the larger is the deviation of the density from $\rho_{D,min}^* \approx 0.31$.

As far as a comparison with previous numerical studies of the LJY_E model is concerned, recent molecular dynamics simulations coupled with SCGLE³¹ determined a rather flat arrest line, located at $T^* \approx 0.1$ for low and moderate densities, and then slightly rising for $\phi \gtrsim 0.3$. This datum (cf. Fig. 15 of Ref. 31) turns out to be in a satisfying qualitative agreement with the shape of the $T_D(\rho)$ locus below T_C in Fig. 9(b); in particular, $T_{D,min}^* \approx 0.115$. Cluster-percolated states were also found at $\phi = 0.125$ ($\rho \approx 0.24$) and $\phi = 0.16$ ($\rho \approx 0.30$),⁵⁸ both states falling within the $\rho_{\times 1}^* - \rho_{\times 2}^*$ interval. Moreover, the experimental percolation line falls at $\rho \approx 0.19$ in the temperature range around $T_{D,min}^* \approx 0.115$,⁵⁷ again in close agreement with our threshold $\rho_{\times 1}^* \approx 0.18$. However, in Ref. 58, percolation is found at $\phi = 0.125$ both at $T^* = 0.2$ and at $T^* = 0.05$, with an intermediate temperature range where the system does not percolate, while for $\phi = 0.16$, percolation is found already at a temperature as high as $T^* = 0.3$, well above our T_C locus. We have found no evidence of such a re-entrant behavior or high-temperature arrested states. With the theoretical tool in use, we are not able to further inquiry into the discrepancies emerging with Ref. 58.

As for the properties of LJY_E within regime I (i.e., for densities lower than $\rho_{\times 1}^*$), we see in Fig. 9(b) that $T_D(\rho)$ turns to be systematically higher than $T_C(\rho)$ or—to be more conservative—higher than the temperature for which $S(q_c) \approx 2.7$. Therefore, as the fluid is cooled down in this dilute regime, clustering is preempted by dynamical arrest. The calculation of $\langle n \rangle$ along $T_D^*(\rho^*)$ for $\rho^* \leq \rho_{\times 1}^*$, reported in Table III, demonstrates how this quantity is systematically higher than $\langle n_0 \rangle = 2.4$, thus confirming our prediction.

Our evidence points to the existence of an unexpected low-density arrested state made of particles, i.e., possibly a glass in which clusters are not the building blocks. Now, it is well recognized that, at a very low density, the fluid is unable to stabilize a cluster fluid, and, therefore, a homogeneous vapor phase persists;²⁰ under these

conditions, it is clear that, whatever the fate of the fluid at low temperatures (attaining either an ergodic or a non-ergodic state),²⁸ its building blocks are represented by single particles. The novelty of our finding is that such an arrested state may take place even upon conditions favorable to clustering.

To summarize, at variance with all models investigated in sections III and IV, the LJY_E exhibits a more complex phase portrait. For example, if we compress the fluid at constant temperature slightly below $T_{C,\max}^*$, we see in Fig. 9(b) that it successively passes from the low-density arrested phase to an IRO state and then to a disordered cluster phase, to fall again in the IRO before eventually entering, at much higher densities, a glassy phase made of particles. In addition, over a narrow temperature range slightly above $T_{C,\max}^*$, there are isotherms along which the fluid first falls into the low-density arrested phase and then traverses a large density interval where clustering is inhibited, to finally end in high-density glass phase.

B. Weakening the repulsive tail

To further elucidate the relationship between phase equilibria and LJY_E features, we study the interplay between $T_C(\rho)$ and $T_D(\rho)$, as the strength of the repulsive Yukawa tail is progressively decreased from $A = 8\epsilon$, with fixed $\alpha = 18$ and $\xi_D = 0.5\sigma$. The four potentials obtained from the original LJY_E with $A/\epsilon = 7.8, 7.3, 6.7$, and 6.5 are shown in Fig. 10(a). We see that the decrease in A within that range has just a moderate effect on the overall shape of the interaction potential: both the attraction depth and the repulsive barrier are slightly reduced, while the range of both contributions remains practically the same.

The phase diagrams are displayed in Fig. 10(b). As for the locus $S(q_c) \approx 2.7$ vs ρ , we see that the bending toward high temperatures in regime I—already discussed for the original LJY_E in Fig. 9(b)—is progressively enhanced as A decreases, until, at $A = 6.7\epsilon$, $T_{C,\min}^*$ disappears in favor of a broad plateau. Therefore, upon compression from very dilute conditions, T_C^* initially decreases, then flattens, and finally decreases again. Eventually, for the even lower $A = 6.5\epsilon$, the observed plateau gives way to a monotonic decrease, possibly indicating that compressing the fluid is detrimental to clustering. As for $T_D(\rho)$, this locus follows the same trend observed for LJY_E, regardless of the value of A , but for a constant shift toward higher temperatures as A decreases. At the same time, $\rho_{D,\min}^*$ moves toward higher densities.

The density of the intersection point between $T_C(\rho)$ and $T_D(\rho)$ on the low-density side, ρ_{x1} , turns out to be remarkably constant with A , signaling the existence of a minimum density threshold for the existence of arrested states made of clusters, practically independent of the specific LJY parameterization. In the range $\rho < \rho_{x1}$, the differences between $T_D(\rho)$ and $T_C(\rho)$ get progressively thinner, until the two loci practically stick together for $A \leq 6.7\epsilon$.

The most important observation is that for $\rho < \rho_{x1}$, $T_D(\rho)$ remains systematically higher than $T_C(\rho)$. This evidence corroborates our predictions concerning the original LJY_E model: an arrested state made of particles is likely to characterize the low-density behavior of a whole family of LJY potentials, preempting the existence of a clustered state.

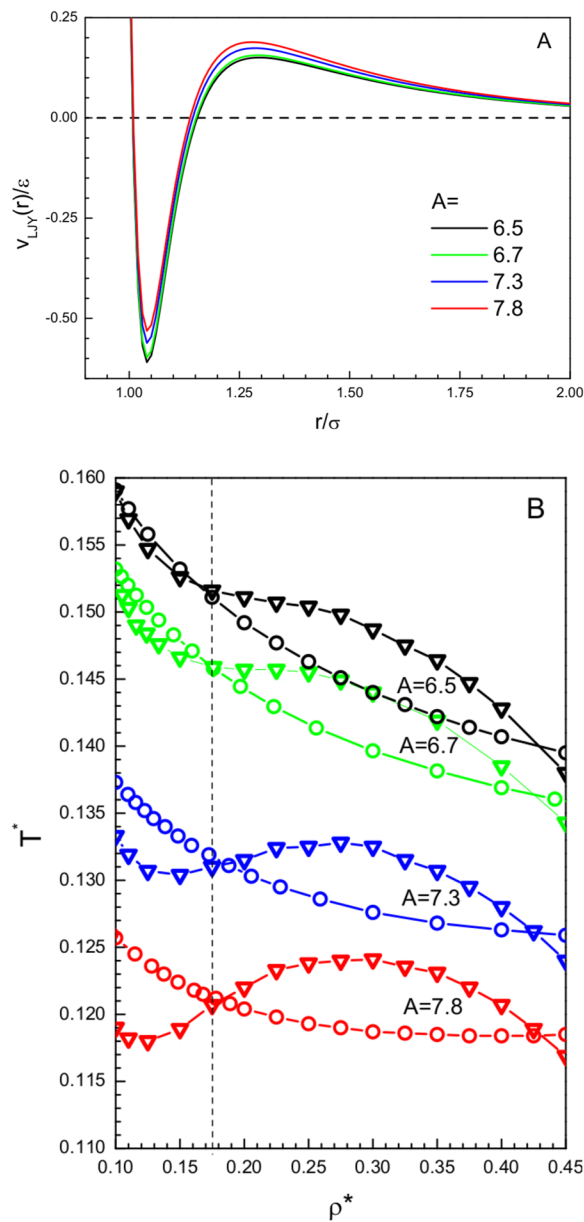


FIG. 10. (a) LJY models with $\alpha = 18$, $\xi_D = 0.5\sigma$, and different strength A (reported in the legend in units of ϵ). We recall that in the original LJY_E, $A = 8\epsilon$. (b) Corresponding phase diagram, in terms of $T_C^*(\rho^*)$ (triangles) and $T_D^*(\rho^*)$ (circles); the vertical dashed line indicates ρ_{x1}^* .

C. Structural properties

The proximity of the $T_D(\rho)$ loci for the LJY_E and LJY(100,0.2,2) models offers the opportunity to discuss and compare the structural properties of both models for selected state points.

In Fig. 11, we show the low- q portion of the structure factors calculated for three different densities, namely $\rho^* = 0.2, 0.3$, and

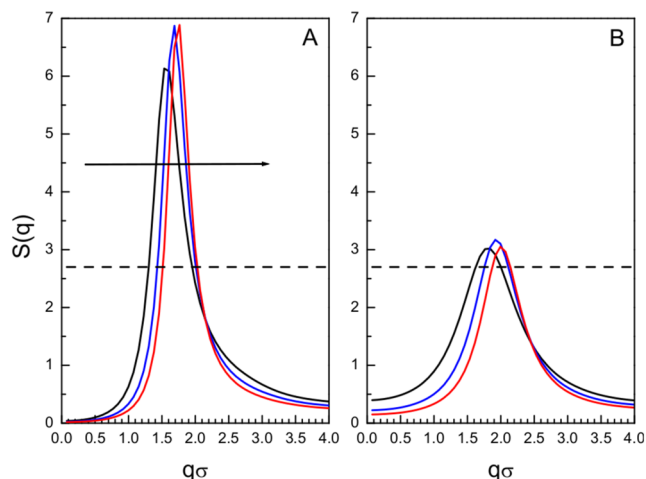


FIG. 11. Structure factors calculated at $\rho^* = 0.2$ (black), 0.3 (blue), and 0.4 (red) and fixed $T^* = 0.11$. (a) LJY(100,0.2,2) and (b) LJY_E. The horizontal dashed lines indicate the threshold $S(q_c) = 2.7$; the arrow in (a) points toward increasing densities.

0.4, and fixed $T^* = 0.11$, all conditions for which both LJY_E and LJY(100,0.2,2) fall deeply within their respective arrested phases; see Fig. 9(b). The presence of a low- q peak in all cases testifies the tendency of particles to aggregate. As seen in (a) [concerning LJY(100,0.2,2)], both $S(q_c)$ and q_c increase with density, indicating that—if the inverse of q_c is assumed to be a measure of the inter-cluster correlation distance—clusters are more disconnected at low densities. The position of the main scattering peak in $S(q)$ (not shown), corresponding to nearest-neighbor correlations, remains unchanged. In (b) (concerning LJY_E), the same trend is observed for q_c but not for $S(q_c)$, showing a maximum at $\rho^* = 0.3$, reminiscent of the concave shape exhibited by $T_C^*(\rho^*)$; see Fig. 9(b).

Even if LJY(100,0.2,2) and LJY_E exhibit arrested states in close ranges of temperature, the nature of such states differs. For instance, $S(q_c)$ is systematically higher for the former model, while the peak locations q_c are nearly the same. This indicates that clusters correlate over similar distances in both fluids, but interact more strongly when the LJY(100,0.2,2) is considered. As for $S(q \rightarrow 0)$, the low values attained for LJY(100,0.2,2) even at the lowest density indicate that the corresponding arrested states are hardly compressible. Meanwhile, a striking feature characterizes $S(q)$ for LJY_E, for which substantially higher values are observed. This evidence is noteworthy, given the typically low compressibility observed in glasses. This propensity originates from the choice $\alpha = 18$ in LJY_E: indeed, low-density state points described through the bare Lennard-Jones potential with the same α are characterized by structure factors with high $S(q = 0)$ values.

To conclude, we show in Fig. 12(a) the evolution of the LJY_E pair correlation function, as the density increases from $\rho^* = 0.1$ to 0.15 and finally to 0.18 (with the latter corresponding to $\rho_{\times 1}^* = 0.18$), along the isotherm $T^* = 0.117$. As visible from Fig. 9(b), all conditions fall within the low-density arrested phase. At $\rho^* = 0.1$, the first peak is sharply defined, and followed by three well distinct coordination shells, testifying that this state point is already ordered at long

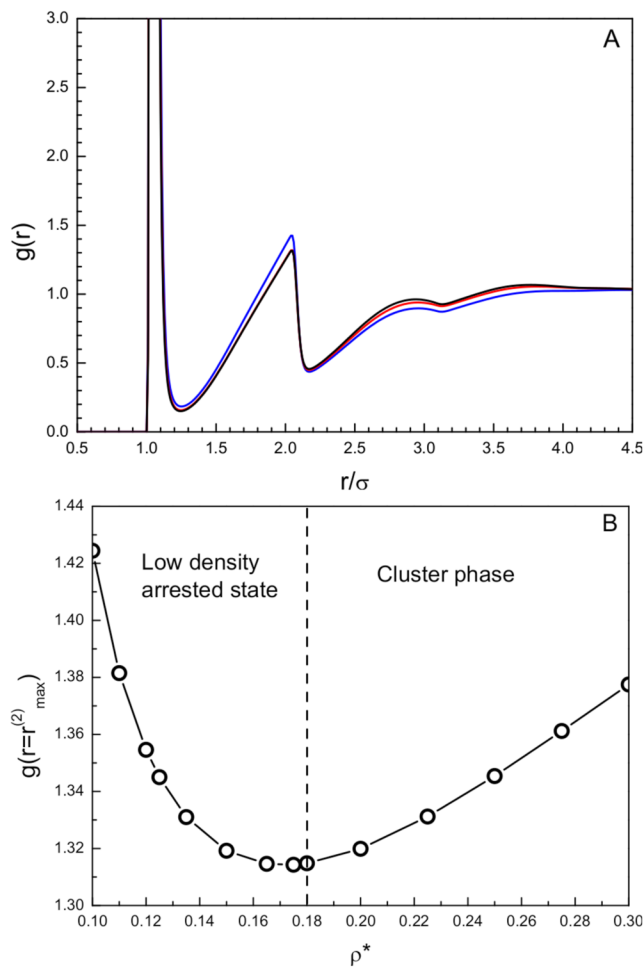


FIG. 12. (a) LJY_E $g(r)$ at $\rho^* = 0.1$ (blue), 0.15 (red), and 0.18 (black), and $T^* = 0.117$. (b) Behavior of the second peak of $g(r)$ vs ρ^* at the same temperature.

distances. We recall that, for classical fluids, the amplitude of successive peaks of $g(r)$ is known to increase upon compression, but this is not the case for the present model. In fact, if the amplitude of the first, third, and fourth peaks is seen to grow with the density, the behavior of the second peak of $g(r)$ —denoted as $g(r_{\max}^{(2)})$, falling at $r_{\max}^{(2)} = 2.05\sigma$ independently of ρ —contrasts with this trend. As seen in Fig. 12(b), upon compression, $g(r_{\max}^{(2)})$ first decreases and then increases, with a minimum exactly falling at $\rho_{\times 1}^* = 0.18$, where, by our definition, the threshold $S(q_c) = 2.7$ is reached. In other words, the observed reversal of trend of $g(r_{\max}^{(2)})$ (concerning local, real-space correlations) and the criterion of Ref. 20 (concerning long-range correlations in the reciprocal space) perfectly agree in indicating the onset of clustering at the state point [$T_C^* = 0.117$, $\rho^* = 0.18$]. This observation confirms, for the LJY_E model at issue, the quality of our local-correlation criterion to identify the clustering threshold,^{22–24} initially proposed for the two-Yukawa SALR model, and therein assessed in a substantially higher density regime.

VI. CONCLUSIONS

The motivation for the present work was twofold: On the one hand, we have been inspired by numerical evidence that systems interacting through very short-range potentials with competing contributions (SALR fluids) may exhibit, at low temperatures and densities, arrested states made of clusters.^{26,27} On the other hand, we wanted to apply for the first time our integral equation implementation of the replica method^{49,52} to detect the arrested states arising in SALR fluids.

The SALR interaction we have used for our purposes is composed of a generalized $(2\alpha, \alpha)$ Lennard-Jones potential and a screened Coulomb potential, accounted for by a repulsive (A, ξ_D) Yukawa term, with A and ξ_D being the strength and the Debye screening length, respectively, whence the name LJY (α, A, ξ_D) .

We have studied a number of different $[\alpha, A, \xi_D]$ sets, resulting in the determination of the low-temperature phase diagrams of as many as 11 LJY models. Each temperature–density phase diagram is composed of the cluster–phase boundary, identified by the locus $T_C(\rho)$ and the arrested-state locus $T_D(\rho)$. Along an isochore, the onset of the cluster phase is signaled by the heuristic criterion $S(q_c) = 2.7$,²⁰ where q_c is the position of the low- q peak in the structure factor. The dynamical-transition temperature T_D is obtained as the highest temperature at which non-trivial solutions of Eqs. (3) and (4) exist. Before tackling the study of LJY models, we have positively assessed our predictions for the standard Lennard-Jones fluid against the more complex implementation of the replica formalism of Ref. 59.

The interplay between $T_C(\rho)$ and $T_D(\rho)$, with these two loci falling alternatively one on top of the other, depending on thermodynamic conditions and interaction parameters, gives rise to a rich variety of arrested states interspersed with non-arrested states, of which either clusters or single particles provide the building blocks.

As for the locus $T_C(\rho)$, this generally exhibits a re-entrant concave shape, with a maximum located at $[\rho_{C,\max}, T_{C,\max}]$; increasing α from 6 to 100, with fixed A and ξ_D , leads to shorter and shorter LJY attractions, with the ensuing decrease of $T_{C,\max}$. As for the locus $T_D(\rho)$, the corresponding arrested states are found all over the range of fluid densities, but for $\alpha = 6$ and 12, for which this locus does not extend to the low-density regime (see e.g., Fig. 2). In this case, the cluster fluid can reach the λ -line, heralding favorable conditions for the development of ordered microphases. Due to its convex shape, $T_D(\rho)$ exhibits a minimum located at $[\rho_{D,\min}, T_{D,\min}]$; however, $T_D(\rho)$ gradually flattens with increasing α , until a slope close to zero is eventually reached for $\alpha = 100$; see Fig. 6(b). At intermediate densities, $T_C(\rho)$ and $T_D(\rho)$ cross each other at $[\rho_\times, T_\times]$, in such a way that for $\rho < \rho_\times$, T_D falls below T_C , and vice versa for $\rho > \rho_\times$; see again Fig. 6(b). Therefore, below T_D , the system is in the (disordered or percolated) cluster phase for $\rho < \rho_\times$, while it is in a (disordered or percolated) arrested phase made of particles at higher densities. Above $T_{D,\min}$, the fluid undergoes successive phase transitions upon compression, alternating arrested and non-arrested states of different nature.

As far as the comparison with simulation results available from other sources is concerned, our predictions for $T_D(\rho)$ in the low-density regime for the set $[\alpha = 100, A = 0.2\epsilon, \xi_D = 2\sigma]$ turn out to be in gratifying agreement with the finite- T arrest line derived

in Ref. 27. Moreover, we have analyzed a realistic LJY colloidal model,^{57,58} with $[\alpha = 18, A = 8\epsilon, \xi_D = 0.5\sigma]$, referred to as LJY_E in the text. Again, in agreement with recent numerical results,³¹ arrested states arise all over the fluid density range.

In conclusion, we are confident about the effectiveness of our simplified static replica approach in providing a unified framework for the study of arrested states occurring in the prototype LJY fluid, irrespective of their nature.

Different possible developments can be foreseen. On the one side, we hope that our theoretical framework will serve as a useful guide for future numerical studies concerning arrested states in SALR fluids. As for our projects, we plan to apply our theoretical approach to predict the arrest properties of other SALR fluids. Moreover, we are lively searching, within our scheme, for possible indicators useful to discriminate between different clustered arrested states. Finally, several outcomes emerging from the present study call for further investigations. For instance, the LJY_E phase diagram in Fig. 9(b) reveals a couple of unexpected features: at low densities, $T_D(\rho)$ falls above $T_C(\rho)$, suggesting the occurrence of a previously undetected arrested phase made of particles, which preempts in this regime the existence of a clustered state. In addition, the $S(q_c) \approx 2.7$ threshold apparently displays a minimum as a function of the density in the same dilute regime. This outcome could represent a breach in the “universal,” roughly parabolic shape of $T_C(\rho)$, well recognized in the literature. Both features certainly deserve a careful numerical assessment, especially because we have found that they affect a whole family of LJY_E models, as obtained from the original one by systematically decreasing the repulsive strength of the Yukawa tail.

ACKNOWLEDGMENTS

The authors thank Professor Jean-Pierre Hansen for fruitful discussion and for a careful reading of the manuscript during all stages of preparation. They also acknowledge the computer time made available at the Pole Messin de Modélisation et Simulation (PMMS) and within the PO-FESR 2007–2013 MedNETNA (Mediterranean Network for Emerging Nanomaterials) Project.

AUTHOR DECLARATIONS

Conflict of Interest

The authors have no conflicts to disclose.

Author Contributions

Jean-Marc Bomont: Conceptualization (lead); Formal analysis (equal); Investigation (lead); Methodology (equal); Software (equal); Writing – original draft (lead); Writing – review & editing (equal). **Giorgio Pastore:** Conceptualization (equal); Methodology (equal); Software (equal); Writing – review & editing (equal). **Dino Costa:** Conceptualization (equal); Methodology (equal); Writing – review & editing (equal). **Gianmarco Munaò:** Conceptualization (equal); Methodology (equal); Writing – review & editing (equal). **Gianpietro Malescio:** Conceptualization (equal); Methodology (equal); Writing – review & editing (equal). **Santi Prestipino:**

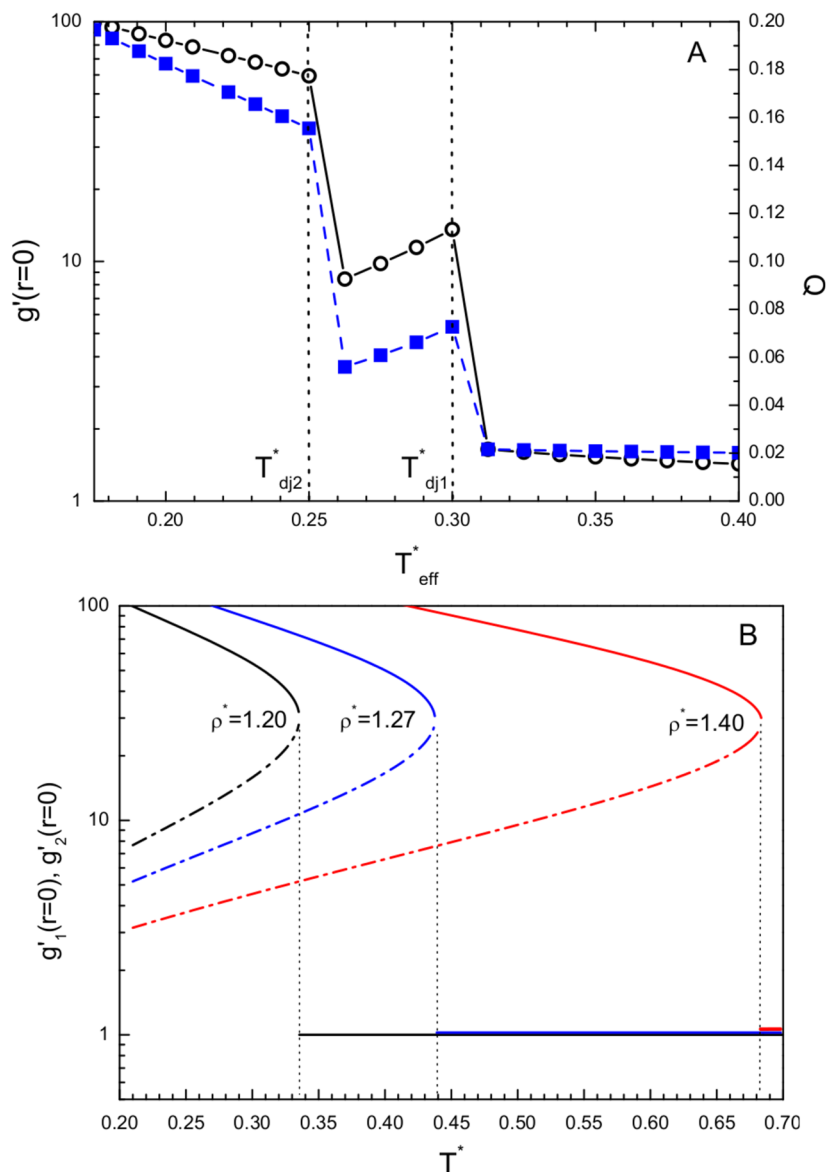


FIG. 13. Standard LJ fluid. (a) Order parameters $g'(0)$ (circles, left scale) and Q (squares, right scale) vs T_{eff}^* at fixed $\rho^* = 1.20$, for $m = 0.8$, $\varepsilon'_0 = 0.1\varepsilon$, and $c = 0.3\sigma$. The two temperatures at which both order parameters change discontinuously, $T_{\text{dj1}}^* = 0.30$ and $T_{\text{dj2}}^* = 0.25$, are also indicated. (b) Order parameters $g'_1(0)$ within G_1 (dotted-dashed lines), $g'_2(0)$ within G_2 (solid lines), and both within the liquid phase (horizontal lines) as a function of temperature, for three densities, in the limits $\varepsilon' \rightarrow 0$ and $m \rightarrow 1$. The corresponding T_D^* values are indicated by the vertical lines.

Conceptualization (equal); Methodology (equal); Writing – review & editing (equal).

DATA AVAILABILITY

The data that support the findings of this study are available from the corresponding author upon reasonable request.

APPENDIX: DYNAMICAL TRANSITION LINE OF THE STANDARD LENNARD-JONES FLUID

We have solved the HNC equations for $g(r)$ and $g'(r)$ with $m = 0.8$ and $\varepsilon'_0 = 0.1\varepsilon$ along three isochores, $\rho^* = 1.20$, 1.27 , and 1.40 . In the work of Mézard and Parisi,^{54,59} the motivation for using $m < 1$ is to allow using a liquid state theory like HNC to describe the molecular fluid at $m < 1$, avoiding the transition at the Kauzmann

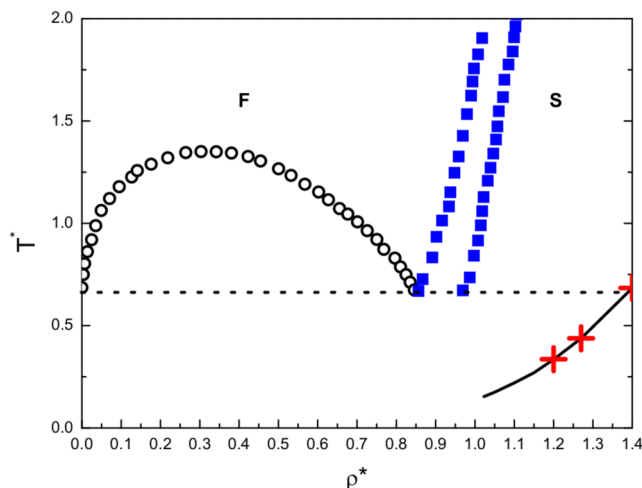


FIG. 14. Dynamical arrest line of LJ fluid (black), as compared with predictions from Ref. 59 (crosses). For completeness, liquid–vapor (circles) and fluid–solid (squares) coexistence points are also shown,⁷⁸ with the dotted line indicating the triple-point temperature.

temperature T_K , where the configurational entropy vanishes. Therefore, we can use the free energy of the molecular liquid to deduce the free energy of the glass phase at $m = 1$. We refer the interested reader to the cited references for full details.

Figure 13(a) illustrates the essential features of the complex Lennard-Jones glassy free energy landscape made of basins and barriers.^{75–77} At the effective temperature $T_{dj1}^* = 0.30$, for $\rho^* = 1.20$, both order parameters $g'(0)$ and Q undergo a first discontinuous jump to much higher values. Going deeper in the glass phase, a second branch of solutions appears discontinuously, at a lower effective temperature $T_{dj2}^* = 0.25$. These jumps signal a broken replica symmetry of the system, a feature that represents the very foundation of the replica method.⁵⁴ Since $g'(0)$ and Q decrease for $T_{dj2}^* < T_{eff}^* < T_{dj1}^*$, the first jump is specific to the G_1 solution. Meanwhile, since $g'(0)$ and Q increase for $T_{eff}^* < T_{dj2}^*$, the second jump is specific to the “ideal” glass phase G_2 .

To recover the properties of the original system, ϵ'_0 is progressively switched off within G_1 and G_2 solutions and the limit $m \rightarrow 1$ is taken thereafter. In this way, non-trivial solutions $g'_1(r)$ and $g'_2(r)$ within G_1 and G_2 phases are obtained and then used to calculate the corresponding overlaps. We remark that, should ϵ'_0 be switched off too hastily—i.e., at $T_{eff}^* > T_{dj1}^*$ —initially paired atoms would drift away from each other in the liquid phase. To investigate the isochores $\rho^* = 1.27$ and 1.40 , we do not need to repeat our search protocol in full, since non-trivial solutions for these two states can simply be obtained by compressing the system at constant temperature from $\rho^* = 1.20$. The search for $T_D(\rho)$ has been carried out for each of the three studied densities. To this aim, each glassy state (ρ^* , T^*) was annealed.

Figure 13(b) shows the variation of $g'_1(0)$ and $g'_2(0)$ with increasing T^* for each density. As is clear, the order parameter increases along the G_1 branch and, vice versa, it decreases along G_2 . For each density, G_1 and G_2 solutions coexist over the same range

of temperatures and end up at the same temperature $T_D^*(\rho^*)$. Above T_D^* , both order parameters drop to their L values $g'_1(0) = g'_2(0) = 1$. The benchmark of the previously undetected G_1 -type solutions is that they are able to predict T_D in the same manner as G_2 -type solutions do. No “glassy” solutions of the HNC equations exist above this temperature, which coincides with the dynamical transition point obtained by Franz *et al.*⁵⁹ for the same model (cf. Table II therein), using a much more elaborate approach.

Finally, we have extended our calculations of the dynamical transition line all over the density range [1.0–1.4]. In Fig. 14, our predictions are embodied in the equilibrium phase diagram of the Lennard-Jones fluid;⁷⁸ therein, the perfect consistency with previous results⁵⁹ can be visually appraised.

REFERENCES

- E. Zaccarelli, *J. Phys.: Condens. Matter* **19**, 323101 (2007).
- Y. Zhuang and P. Charbonneau, *J. Phys. Chem. B* **120**, 6178 (2016).
- E. Zaccarelli, “Colloidal arrested states of matter” in *Proceedings of the International School of Physics ‘Enrico Fermi,’ Course CLXXXIV on ‘Physics of Complex Colloids,’* edited by C. Bechinger, F. Sciortino, and P. Zihler (IOS, SIF, Amsterdam, Bologna, 2013).
- M. Bini, G. Brancolini, and V. Tozzini, *Front. Mol. Biosci.* **9**, 986223 (2022).
- J.-M. Bomont, *Adv. Chem. Phys.* **139**, 1 (2008).
- J.-P. Hansen and I. R. McDonald, *Theory of Simple Liquids*, 4th ed. (Academic Press, Oxford, 2013).
- R. P. Sear and W. M. Gelbart, *J. Chem. Phys.* **110**, 4582 (1999).
- Y. Liu and Y. Xi, *Curr. Opin. Colloid Interface Sci.* **39**, 123 (2019).
- J. Ruiz-Franco and E. Zaccarelli, *Annu. Rev. Condens. Matter Phys.* **12**, 51 (2021).
- L. L. Lee *et al.*, *J. Chem. Phys.* **132**, 074505 (2010).
- J.-M. Bomont, J.-L. Bretonnet, and D. Costa, *J. Chem. Phys.* **132**, 184508 (2010).
- J. M. Kim, R. Castañeda-Priego, Y. Liu, and N. J. Wagner, *J. Chem. Phys.* **134**, 064904 (2011).
- J.-M. Bomont, J. L. Bretonnet, D. Costa, and J. P. Hansen, *J. Chem. Phys.* **137**, 011101 (2012).
- J.-M. Bomont and D. Costa, *J. Chem. Phys.* **137**, 164901 (2012).
- G. Cigala, D. Costa, J. M. Bomont, and C. Caccamo, *Mol. Phys.* **113**, 2583 (2015).
- J. A. Bollinger and T. M. Truskett, *J. Chem. Phys.* **145**, 064903 (2016).
- R. Perdomo-Pérez *et al.*, *J. Phys.: Condens. Matter* **34**, 144005 (2022).
- A. J. Archer and N. B. Wilding, *Phys. Rev. E* **76**, 031501 (2007).
- Y. Liu *et al.*, *J. Phys. Chem. B* **115**, 7238 (2011).
- P. D. Godfrin, N. E. Valadez-Pérez, R. Castañeda-Priego, N. J. Wagner, and Y. Liu, *Soft Matter* **10**, 5061 (2014).
- J.-P. Hansen and L. Verlet, *Phys. Rev.* **184**, 151 (1969).
- J.-M. Bomont, D. Costa, and J.-L. Bretonnet, *Phys. Chem. Chem. Phys.* **19**, 15247 (2017).
- J.-M. Bomont, D. Costa, and J.-L. Bretonnet, *Phys. Chem. Chem. Phys.* **22**, 5355 (2020).
- J.-M. Bomont, D. Costa, and J.-L. Bretonnet, *AIMS Mater. Sci.* **7**, 170 (2020).
- J. Bosse and S. D. Wilke, *Phys. Rev. Lett.* **80**, 1260 (1998).
- F. Sciortino, S. Mossa, E. Zaccarelli, and P. Tartaglia, *Phys. Rev. Lett.* **93**, 055701 (2004).
- J. C. F. Toledano, F. Sciortino, and E. Zaccarelli, *Soft Matter* **5**, 2390 (2009).
- C. L. Klix, C. P. Royall, and H. Tanaka, *Phys. Rev. Lett.* **104**, 165702 (2010).
- W. Götze, *Complex Dynamics of Glass-Forming Liquids: A Mode Coupling Theory* (Oxford University Press, New York, 2009).
- J. Wu, Y. Liu, W. R. Chen, J. Cao, and S. H. Chen, *Phys. Rev. E* **70**, 050401 (2004).
- A. Torres-Carbajal and P. E. Ramirez-González, *J. Phys.: Condens. Matter* **34**, 224002 (2022).
- A. G. Carretas-Talamante *et al.*, *J. Chem. Phys.* **158**, 064506 (2023).

- ³³R. Juárez-Maldonado and M. Medina-Noyola, *Phys. Rev. E* **77**, 051503 (2008).
- ³⁴L. Yeomans-Reyna *et al.*, *Phys. Rev. E* **76**, 041504 (2007).
- ³⁵J. B. Zepeda-López and M. Medina-Noyola, *J. Chem. Phys.* **154**, 174901 (2021).
- ³⁶J. M. Olais-Govea, L. López-Flores, and M. Medina-Noyola, *J. Chem. Phys.* **143**, 174505 (2015).
- ³⁷M. A. Chávez-Rojo and M. Medina-Noyola, *Phys. Rev. E* **72**, 031107 (2005).
- ³⁸S. Franz and G. Parisi, *J. Phys. I* **5**, 1401 (1995).
- ³⁹S. Franz and G. Parisi, *Phys. Rev. Lett.* **79**, 2486 (1997).
- ⁴⁰S. Franz and G. Parisi, *Physica A* **261**, 317 (1998).
- ⁴¹L. Berthier and G. Biroli, *Rev. Mod. Phys.* **83**, 587 (2011).
- ⁴²B. Guiselin, L. Berthier, and G. Tarjus, *SciPost Phys.* **12**, 091 (2022).
- ⁴³L. Berthier, *Phys. Rev. E* **88**, 022313 (2013).
- ⁴⁴G. Parisi and B. Seoane, *Phys. Rev. E* **89**, 022309 (2014).
- ⁴⁵R. M. Turner, R. L. Jack, and J. P. Garrahan, *Phys. Rev. E* **92**, 022115 (2015).
- ⁴⁶J.-M. Bomont, G. Pastore, and J.-P. Hansen, *Europhys. Lett.* **105**, 36003 (2014).
- ⁴⁷J.-M. Bomont, J.-P. Hansen, and G. Pastore, *J. Chem. Phys.* **141**, 174505 (2014).
- ⁴⁸J.-M. Bomont and G. Pastore, *Mol. Phys.* **113**, 2770 (2015).
- ⁴⁹J.-M. Bomont, J.-P. Hansen, and G. Pastore, *Phys. Rev. E* **92**, 042316 (2015).
- ⁵⁰J.-M. Bomont, J.-P. Hansen, and G. Pastore, *Adv. Comput. Sci.* **7**, 108 (2017).
- ⁵¹J.-M. Bomont, G. Pastore, and J. P. Hansen, *J. Chem. Phys.* **146**, 114504 (2017).
- ⁵²J.-M. Bomont, J.-P. Hansen, and G. Pastore, *J. Chem. Phys.* **150**, 154504 (2019).
- ⁵³J.-M. Bomont, C. N. Likos, and J.-P. Hansen, *Phys. Rev. E* **105**, 024607 (2022).
- ⁵⁴M. Mézard and G. Parisi, *J. Chem. Phys.* **111**, 1076 (1999).
- ⁵⁵R. Monasson, *Phys. Rev. Lett.* **75**, 2847 (1995).
- ⁵⁶G. A. Vliegthart *et al.*, *Physica A* **263**, 378 (1999).
- ⁵⁷A. I. Campbell, V. J. Anderson, J. S. van Duijneveldt, and P. Bartlett, *Phys. Rev. Lett.* **94**, 208301 (2005).
- ⁵⁸F. Sciortino, P. Tartaglia, and E. Zaccarelli, *J. Phys. Chem. B* **109**, 21942 (2005).
- ⁵⁹S. Franz, H. Jacquin, G. Parisi, P. Urbani, and F. Zamponi, *J. Chem. Phys.* **138**, 12A540 (2013).
- ⁶⁰E. Mani, W. Lechner, W. K. Kegel, and P. G. Bolhuis, *Soft Matter* **10**, 4479 (2014).
- ⁶¹W. E. J. Verwey and J. T. G. Overbeek, *Theory of the Stability of Lyophobic Colloids* (Dover Publications, Mineola, NY, 1999).
- ⁶²M. Mézard and G. Parisi, *Glasses and Replicas* (John Wiley and Sons, New-York, 2012), Chap.4, pp. 151–191.
- ⁶³M. Broccio, D. Costa, Y. Liu, and S.-H. Chen, *J. Chem. Phys.* **124**, 084501 (2006).
- ⁶⁴I. Guillén-Escamilla, J. G. Méndez-Bermúdez, J. C. Mixteco-Sánchez, and G. A. Méndez-Maldonado, *Rev. Mex. Fis.* **68**, 050502 (2022).
- ⁶⁵D. Costa, G. Munaò, J.-M. Bomont, G. Malescio, A. Palatella, and S. Prestipino, *Phys. Rev. E* **108**, 034602 (2023).
- ⁶⁶G. Parisi and F. Zamponi, *Rev. Mod. Phys.* **82**, 789 (2010).
- ⁶⁷M. J. Gillan, *Mol. Phys.* **38**, 1781 (1979).
- ⁶⁸L. Belloni, *J. Chem. Phys.* **98**, 8080 (1993).
- ⁶⁹S. Mossa, F. Sciortino, P. Tartaglia, and E. Zaccarelli, *Langmuir* **20**, 10756 (2004).
- ⁷⁰J. C. Phillips, *J. Non-Cryst. Solids* **34**, 153 (1979).
- ⁷¹N. E. Valadez-Pérez *et al.*, *Phys. Rev. E* **88**, 060302(R) (2013).
- ⁷²M. G. Noro and D. Frenkel, *J. Chem. Phys.* **113**, 2941 (2000).
- ⁷³G. Zerah and J.-P. Hansen, *J. Chem. Phys.* **84**, 2336 (1986).
- ⁷⁴J. D. Weeks, D. Chandler, and H. C. Andersen, *J. Chem. Phys.* **54**, 5237 (1971).
- ⁷⁵T. R. Kirkpatrick and P. G. Wolynes, *Phys. Rev. B* **36**, 8552 (1987).
- ⁷⁶T. R. Kirkpatrick and D. Thirumalai, *Phys. Rev. Lett.* **58**, 2091 (1987).
- ⁷⁷*Structural Glasses and Supercooled Liquids: Theory, Experiment, and Applications*, edited by P. Wolynes and V. Lubchenko (John Wiley and Sons, New-York, 2012).
- ⁷⁸See https://en.wikipedia.org/wiki/Lennard-Jones_potential for information about the phase diagram of the Lennard-Jones fluid.